Neurosci. Bull. December, 2023, 39(12):1762–1774
https://doi.org/10.1007/s12264-023-01069-y

www.neurosci.cn
www.springer.com/12264

ORIGINAL ARTICLE

Fgf8$^{P2A\text{-}3\times GFP/+}$: A New Genetic Mouse Model for Specifically Labeling and Sorting Cochlear Inner Hair Cells

Yi Pan[1] · Shuting Li[2,3] · Shunji He[2] · Guangqin Wang[2,3] · Chao Li[2] · Zhiyong Liu[2,4] · Mingliang Xiang[1]

Received: 29 December 2022 / Accepted: 8 March 2023 / Published online: 26 May 2023

Abstract The cochlear auditory epithelium contains two types of sound receptors, inner hair cells (IHCs) and outer hair cells (OHCs). Mouse models for labelling juvenile and adult IHCs or OHCs exist; however, labelling for embryonic and perinatal IHCs or OHCs are lacking. Here, we generated a new knock-in *Fgf8*$^{P2A\text{-}3\times GFP/+}$ (*Fgf8*$^{GFP/+}$) strain, in which the expression of a series of three GFP fragments is controlled by endogenous *Fgf8 cis*-regulatory elements. After confirming that GFP expression accurately reflects the expression of *Fgf8*, we successfully obtained both embryonic and neonatal IHCs with high purity, highlighting the power of *Fgf8*$^{GFP/+}$. Furthermore, our fate-mapping analysis revealed, unexpectedly, that IHCs are also derived from inner ear progenitors expressing *Insm1*, which is currently regarded as an OHC marker. Thus, besides serving as a highly favorable tool for sorting early IHCs, *Fgf8*$^{GFP/+}$ will facilitate the isolation of pure early OHCs by excluding IHCs from the entire hair cell pool.

Keywords Fgf8 · Inner Hair Cell · Inner Ear · Cochlea

Introduction

Multiomic sequencing and genetic or epigenetic analyses are being increasingly applied in diverse biological studies [1]. To obtain high-quality data in such studies, cell-type-specific analysis is invariably required, and for labeling specific cell subtypes, genetic methods are a widely-used and reproducible solution [2–5]. As in the case of other organs, multiomic analyses have recently been applied to the cochlea [1, 6–10]. The cochlea harbors two subtypes of sound receptor hair cells (HCs), inner HCs (IHCs) and outer HCs (OHCs) [11–13]. Near the IHCs and OHCs are various subtypes of supporting cells (SCs) [14]. During cochlear development, IHCs, OHCs, and SCs are all derived from Atoh1+ progenitor cells [15–17], with the key difference between the cells being that SCs show only low *Atoh1* mRNA expression and HCs show high *Atoh1* mRNA and protein expression [18–20]. Accordingly, *Atoh1* $^{-/-}$ mice lose all HCs and, furthermore, exhibit defective SC development [21–23].

IHCs and OHCs share several general HC characteristics and co-express numerous pan-HC markers, including Myo6 and Myo7a [24]; however, IHCs and OHCs also differ in multiple aspects, as highlighted by their distinct transcriptomic profiles [25–27]. OHCs act as sound amplifiers *via* the unique motor protein Prestin (encoded by *Slc26a5*) [28–30], and IHCs behave as the primary sound receptors that form synapses with spiral ganglion neurons (SGNs) [31–34],

Yi Pan and Shuting Li contributed equally to this work.

Supplementary Information The online version contains supplementary material available at https://doi.org/10.1007/s12264-023-01069-y.

✉ Zhiyong Liu
Zhiyongliu@ion.ac.cn

✉ Mingliang Xiang
xml12128@rjh.com.cn

1 Department of Otolaryngology and Head and Neck Surgery, Ruijin Hospital, Shanghai Jiao Tong University School of Medicine, Shanghai 200025, China

2 Institute of Neuroscience, State Key Laboratory of Neuroscience, CAS Center for Excellence in Brain Science and Intelligence Technology, Chinese Academy of Sciences, Shanghai 200031, China

3 University of Chinese Academy of Sciences, Beijing 100049, China

4 Shanghai Center for Brain Science and Brain-Inspired Intelligence Technology, Shanghai 201210, China

and relative to OHCs, IHCs specifically express vGlut3 (*Slc17a8*) and Otoferlin [35–37]. Moreover, Insm1 is the first transcription factor (TF) that is specifically expressed in nascent OHCs at embryonic day 15.5 (E15.5) in a basal-to-apical and medial-to-lateral gradient across the cochlear duct [38], and although *Insm1* is only transiently expressed in nascent OHCs, the TF is required to consolidate the OHC fate: half or slightly less than half of the OHCs tend to transdifferentiate into IHCs in the absence of Insm1 [39]. Furthermore, OHCs are dysfunctional and show decreased expression of the OHC marker Prestin in $Ikzf2^{cello/cello}$ mutant mice [40]. Notably, unlike Insm1 expression, which is turned off by postnatal day 1 (P1) in OHCs [38], the expression of Ikzf2 is turned on around P4 and maintained permanently thereafter in OHCs [26, 40]. By contrast, a third TF, Tbx2, is expressed in IHCs but not OHCs, and opposite to what has been reported in Insm1 and Ikzf2 mutants, embryonic, neonatal, and adult IHCs tend to transform into OHCs upon conditional deletion of *Tbx2* [26, 41, 42].

Despite the insights offered by the studies noted above, how the initial differences between nascent IHCs and OHCs appear is poorly elucidated and remains a challenging but critical unanswered question in hearing research. One hurdle faced in addressing this question is the lack of a powerful genetic mouse model for specifically labeling IHCs or OHCs for deep sequencing (smart-seq or bulk-seq), particularly at late embryonic and neonatal ages. Here, we exploited the unique expression pattern of fibroblast growth factor 8 (Fgf8), an IHC marker expressed at E15 [43–45], to generate a new mouse model: $Fgf8^{P2A\text{-}3\times GFP/+}$ ($Fgf8^{GFP/+}$ in short). We first confirmed that the expression of GFP generally matches that of *Fgf8* in early embryos, and then showed that the GFP expression is unfailingly limited to IHCs within the cochlea. More importantly, the new model allowed us to successfully obtain pure IHCs at E15.5 and P1 through cell sorting, and we confirmed the purity of the IHCs by using qPCR. To the best of our knowledge, the $Fgf8^{GFP/+}$ mouse is the first genetic model that enables the labeling or sorting of IHCs at embryonic and perinatal ages, and we believe that this model will facilitate future multi-omic analyses of nascent IHCs.

Materials and Methods

Mouse Strains

The $Fgf8^{P2A\text{-}3\times GFP}$ ($Fgf8^{GFP/+}$) knock-in C57BL/6 mouse strain was generated by injecting a single-guide RNA (sgRNA) against *Fgf8*, donor DNA (Fig. 2B), and *Cas9* mRNA into one-cell-stage mouse zygotes. The *Fgf8* sgRNA (*5′-AGCTGGGCGAGCGCCTATCG-3′*) carrying the PAM sequence *GGG* targeted the site immediately before the *Fgf8* stop codon. Founder 0 (F0) mice with potentially correct gene targeting were screened using tail-DNA PCR and then crossed with wild-type (WT) C57BL/6J mice to produce germ-line-stable Founder 1 (F1) mice. The F1 mice were subjected to a second round of tail-DNA PCR and Southern blotting (Fig. 2D and E), and, ultimately, a single F1 mouse without random insertion of the donor DNA in the genome was selected for further breeding. Southern blotting was applied as described in our previous report [4]. The nucleotide sequences of the primers used for tail-DNA PCR were the following: F: *5′-GCCAAGTACGAGGGCTGGTA-3′*; R1: *5′-TGCTCACCATAGGTCCAGGGTT-3′*; R2: *5′-TTCAGGAGAACAGACCAGAGAGCC-3′*. All primers were used concurrently, and the PCR protocol used was 95°C for 3 min, followed by 31 cycles of 95°C for 30 s, 60°C for 40 s, and 72°C for 30 s, and then 72°C for an additional 10 min.

The $Insm1^{GFPCre/+}$ strain was obtained from Mutant Mouse Resource and Research Center (036986-JAX); detailed information on how the strain was generated and genotyped has been described previously [46]. Rosa26-LSL-Tdtomato/+ (Ai9; Jax#: 007909) mice were from The Jackson Laboratory. To check embryonic ages, female mice were crossed at 5 p.m. and the next morning was defined as E0.5 if vaginal plugs were observed. All mice used in this study were bred and raised in SPF-level animal rooms, and animal procedures complied with the guidelines (NA-032 2019) of the Institutional Animal Care & Use Committee of the Institute of Neuroscience (ION), CAS Center for Excellence in Brain Science and Intelligence Technology, Chinese Academy of Sciences.

Sample Processing and Immunofluorescence

Mouse embryos were immersed in fresh 4% paraformaldehyde (PFA; P6148, Sigma) at room temperature for 2 h, after which inner ear tissues were carefully dissected out and further incubated in 4% PFA overnight at 4°C. In the case of mice at postnatal ages, the heart was perfused first with 1× PBS (10 mmol/L phosphate-buffered saline, pH 7.4; E607016-0500, Sangon Biotech) and then with 4% PFA before dissecting out the inner ear, and on the following morning, the inner ear tissues were washed with 1× PBS and subjected to the whole-mount labeling procedure. For inner ear samples from mice older than P7, an additional step of decalcification in 120 mmol/L EDTA at room temperature was required to soften the tissue. The entire cochlear duct was divided into three portions, the base, middle, and apex. To analyze frozen sections (14 μm thick), the inner ear samples were first soaked in 30% sucrose (V900116, Sigma) overnight at 4°C before final embedding in OCT (4583, Sakura) on dry ice.

Both whole-mount samples and frozen sections were permeabilized and blocked at room temperature in a solution I

containing 5% bovine serum albumin (BSA; BP1605-100, Fisher Scientific) and 1% Triton X-100 (X100, Sigma) in 1× PBS for 1 h. Tissues or sections were next incubated with primary antibodies in solution II containing 5% BSA and 0.1% Triton X-100 in 1×PBS overnight at 4°C. Subsequently, the cochlear tissues or inner ear sections were incubated with secondary antibodies in solution II for 4 h, washed thrice with 1× PBS, and counterstained with Hoechst 33342 (1:1000, H3570, Thermo Scientific) in 1× PBS for 2 min at room temperature. Lastly, samples were mounted in ProLong Gold antifade reagent (P36930, Thermo Scientific). The following primary antibodies were used: anti-GFP (chicken, 1:1000, ab13970, Abcam), anti-myosin VII (rabbit, 1:500, 25-6790, Proteus Bioscience), anti-myosin VI (rabbit, 1:500, 25-6791, Proteus Bioscience), and anti-Sox2 (goat, 1:500, sc-17320, Santa Cruz). The secondary antibodies were donkey anti-chicken Alexa Fluor 488 (1:500, 703-545-155, Jackson), donkey anti-rabbit Alexa Fluor 568 (1:500, A10042, Thermo Scientific), donkey anti-rabbit Alexa Fluor 647 (1:500, A31573, Thermo Scientific), and donkey anti-goat Alexa Fluor 647 (1:500, A21447, Thermo Scientific). Samples were scanned at 10× and 60× magnification under a Nikon C2 or Nikon NiE-A1 plus confocal microscope, and all digital images were analyzed and processed using ImageJ. At each age, at least three biological replicates were included in the analysis.

Cell Counting and Quantification

For the cell counts related to Fig. 1, in each turn, an ~200 μm region of the cochlear sensory epithelium was selected under a confocal 60× high-resolution lens, and within the same region, all Tdtomato$^+$ OHCs, IHCs, and SCs (Deiters' cells and pillar cells) were counted. The sensory region was defined by Myo6 staining, and whereas IHCs and OHCs were defined by the Myo6 signal and the location of the cells, Deiters' cells and pillar cells were defined by their location (underneath and near OHCs and IHCs), and the absence of Myo6 staining. The percentage of Tdtomato$^+$ cells of each cell type was calculated by normalizing the number of Tdtomato$^+$ cells against the total number of cells of each type. For statistical analyses, using GraphPad Prism 8.0, we applied one-way ANOVA followed by Student's *t* test with Bonferroni correction. Data are presented as the mean ± SEM.

Sorting GFP$^+$ Cochlear IHCs and Quantitative Real-time PCR Analysis

Cochlear sensory epithelial tissues including IHCs and OHCs of *Fgf8*$^{GFP/+}$ mice at E15.5 and P1 were carefully dissected out and digested in fetal bovine serum (FBS)-free choline chloride solution containing papain (LK003150, Worthington) for 15 min at 37°C. Next, the cochlear samples were further digested in choline chloride solution containing protease (P5147, Sigma) and dispase (LS02104, Worthington) at 1 mg/mL for 20 min at 25°C. The components of the choline chloride solution and the details of the methods used to prepare the final single-cell suspension are described in our previous report [10]. The single-cell suspensions were filtered through a 30 μm cell strainer (130-098-458, Miltenyi), the supernatant was removed by centrifugation at 500× *g* for 3 min, and the cells were resuspended in 500 μL of the choline chloride solution (containing 2% FBS) for sorting using a flow cytometer (MoFlo Astrios EQ). GFP$^+$ cells were sorted and ~50 cells were collected into each tube (containing 10 μL of extraction buffer) for one biological replicate at each age.

Total RNA was extracted using a PicoPure RNA isolation kit (Thermo Scientific, KIT0204), and cDNA was generated using an Ovation RNA-seq system V2 (Tecan Genomics, 7102-32). RT-qPCR was performed using the SYBR Green JumpStart Taq Ready-Mix Kit (S4438-500RXN, Sigma) and samples were run on a Roche 480II qPCR machine. All qPCR primers were pre-tested using standard-curve analysis, and the amplification efficiency was found to be between 0.9 and 1.1. The primers were pre-mixed to 2.0 ng/μL. Table S1 lists the primer sequences.

Single-Molecule Fluorescence *in situ* Hybridization (smFISH) Analysis with the *Fgf8* Probe

The DNA template used for synthesizing the *Fgf8* probe was from Dr. Hai Song (Zhejiang University); the probe sequence is listed in Table S2. Briefly, the *Fgf8* probe sequence was transcribed using T7 RNA polymerase (P2075, Promega) and labeled using a digoxigenin labeling kit (11277073910, Roche). The smFISH procedures used here followed the protocol detailed previously [47].

Auditory Brainstem Response (ABR) Measurement

ABR measurements were made in WT, *Fgf8*$^{GFP/+}$, and *Fgf8*$^{GFP/GFP}$ mice at P42 using the following sound frequencies (in kHz): 4, 5.6, 8, 11.3, 16, 22.6, and 32 (Fig. 2I). Stimulus levels started at 90 dB SPL and descended in 5 dB SPL steps, as we previously described [4, 48, 49]. The ABR wave I amplitude measured from three frequency regions (8, 16, and 32 kHz) was calculated as the difference between the wave I peak and the waveform baseline. Student's *t* test was applied (using GraphPad Prism 8.0) to check for statistical differences at each frequency. Both male and female mice were tested for ABR.

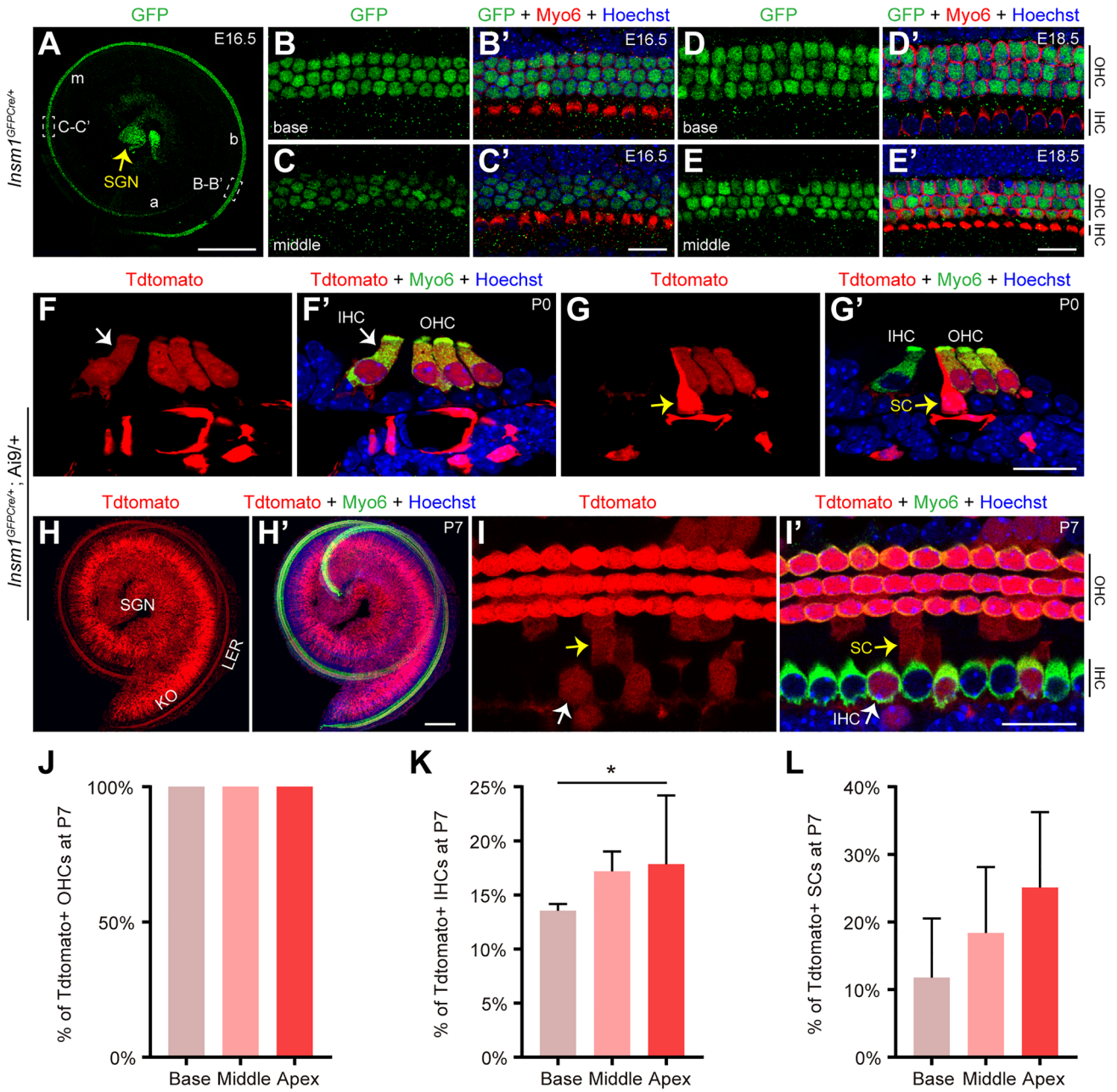

Fig. 1 The progeny of Insm1^{+} precursors includes IHCs and SCs in addition to OHCs. **A–E'** Dual labeling for GFP and the HC marker Myo6 in whole-mount cochlear samples from *Insm1*$^{GFPCre/+}$ mice at E16.5 (**A–C'**) and E18.5 (**D–E'**). Dotted regions in **A** are shown at high resolution in **B–B'**, basal turn, and **C–C'**, middle turn, GFP (Insm1) is expressed in OHCs but not IHCs, and the GFP (Insm1) level in the base is higher than in the middle at E16.5, but the gradient no longer exists at E18.5. **F–I'** Fate-mapping analysis of *Insm1*$^{GFPCre/+}$; Ai9/+ mice at P0 (**F–G'**) and P7 (**H–I'**). All OHCs are Tdtomato^{+}, as expected, and furthermore, Tdtomato^{+} IHCs and SCs are also detected, marked by white and yellow arrows in **F–G'** and **I–I'**, respectively. Low-magnification images in **H** and **H'** show the presence of numerous Tdtomato+ signals in the SGN, KO (Kölliker's organ), and LER (lesser epithelial ridge) regions. **J–L** Quantification of Tdtomato+ OHCs (**J**), IHCs (**K**), and SCs (**L**) at P7. Data are presented as the mean ± SEM (n = 3); *P <0.05 (Student's t test). SGN: spiral ganglion neuron; OHC: outer hair cell; IHC: inner hair cell; SC: supporting cell. Scale bars, 200 μm (**A, H'**); 20 μm (**C', E', G', I'**).

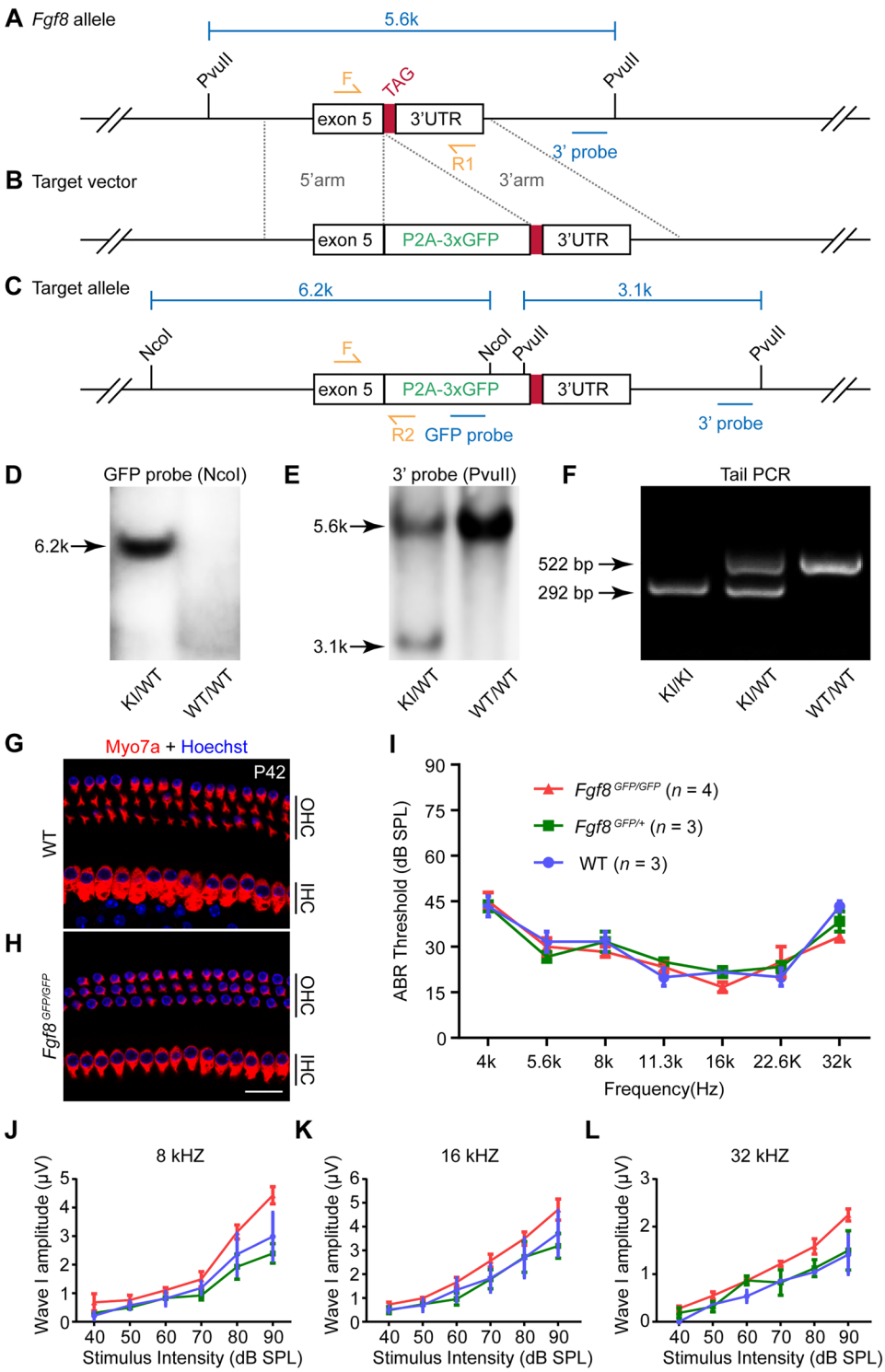

Fig. 2 Generation of the *Fgf8*$^{GFP/+}$ knock-in mouse model. **A–C** In the wild-type *Fgf8* locus (**A**), the fragment containing P2A-3×GFP (**B**) is inserted immediately before the stop codon (GGG), generating the post-targeted allele of *Fgf8* (**C**). **D–E** Southern blotting with internal GFP probe (**D**) and external probe (**E**). The 6.2 kb GFP probe band is detected in the genomic DNA extracted from heterozygous mice (KI/WT) but not wild-type mice (WT/WT); conversely, the 5.6 kb band is detected in the genomic DNA from both KI/WT and WT/WT mice, and the 3.1 kb band is detected only in the KI/WT genomic DNA. **F** Representative agarose-gel image used to distinguish homozygous (KI/KI), heterozygous (KI/WT), and wild-type (WT/WT) mice. **G–H** Immunostaining for the pan-HC marker Myo7a in WT (**G**) and homozygous *Fgf8*$^{GFP/GFP}$ (**H**) mice at P42. **I** ABR measurements from WT (blue, $n = 3$), *Fgf8*$^{GFP/+}$(green, $n = 3$), and *Fgf8*$^{GFP/GFP}$ (red, $n = 4$) mice at P42. **J–L** Wave I amplitudes at 8 (**J**), 16 (**K**), and 32 (**L**) kHz. ABR thresholds and wave I amplitudes do not differ significantly among the three groups (Student's *t* test); data are presented as the mean ± SEM. Scale bar, 20 μm (**H**).

Results

The *Insm1*$^{GFPCre/+}$ Mouse Model Shows Labeling of 13.5%−17.9% of Cochlear IHCs

A previous study reported that OHCs express both Insm1 and Atoh1, whereas IHCs express only Atoh1 [39], and thus the *Insm1*$^{GFPCre/+}$; Ai9/+; *Atoh1*$^{EGFP/+}$ model has been used to sort OHCs and IHCs at P0 [39]. In this model, all OHCs express both EGFP (from *Atoh1*$^{EGFP/+}$) and Tdtomato (from lineage-tracing by *Insm1*$^{GFPCre/+}$; Ai9/+), but IHCs should express only EGFP and, accordingly, should

be EGFP+/Tdtomato- [39]. Moreover, the GFPCre fusion-protein sequence replaces the Insm1 coding sequence in the $Insm1^{GFPCre/+}$ model, and thus $Insm1^{GFPCre}$ is also a null allele [46], and EGFP is fused with the C-terminus of Atoh1 in $Atoh1^{EGFP/+}$ mice [50].

We first independently characterized the $Insm1^{GFPCre/+}$ strain [46]. In addition to confirming that Insm1 is enriched in OHCs, we made certain unexpected observations, as described below. Dual labeling for GFP and the HC marker Myo6 showed that GFP was expressed in OHCs, but not in IHCs, at E16.5 (Fig. 1A–C') and E18.5 (Fig. 1D–E'). GFP was also expressed in cochlear SGN regions (yellow arrow in Fig. 1A), in agreement with the previous report [38]. Moreover, fate-mapping analysis of $Insm1^{GFPCre/+}$; Ai9/+ mice revealed that all OHCs were Tdtomato$^+$, as shown by the dual labeling for Tdtomato and Myo6 at P0 (Fig. 1F–G') and P7 (Fig. 1H–J). Intriguingly, however, Tdtomato+ IHCs (white arrows in Fig. 1F–F', I–I') and SCs (yellow arrows in Fig. 1G–G', I–I') were also frequently captured here: 13.5% ± 0.6%, 17.2% ± 1.8%, and 17.9% ± 6.4% of the IHCs were Tdtomato$^+$ at the basal, middle, and apical turns, respectively, at P7 ($n = 3$, Fig. 1K), and 11.8% ± 8.8%, 18.4% ± 9.7%, and 25.1% ± 11.2% of the cochlear SCs were Tdtomato$^+$ at, respectively, the base, middle, and apex ($n = 3$, Fig. 1L). Numerous Tdtomato$^+$ cells were also detected in the SGN region, which was not the focus of this study.

The Tdtomato$^+$ IHCs and SCs were likely present due to broader Cre activity (visualized using Tdtomato) than previously estimated using the less-sensitive LacZ reporter [38], as revealed by our fate-mapping analysis of $Insm1^{GFPCre/+}$; Ai9/+ embryos at E9.5 (Fig. S1A–C'''). The GFP (Insm1)$^+$ cells that tended to migrate out of the ventral otic epithelium were otic neuroblasts (arrows in Fig. S1D–D'''). Notably, these otic neuroblasts did not express Tdtomato, which suggested that Insm1 expression had just commenced and that the cells would be found to express Tdtomato if analyzed at E10.5. Unexpectedly, the cells distributed in the relatively dorsal/lateral portion of the otocyst were Tdtomato$^+$ (arrows in Fig. S1C–C'''). We speculate that these cells might contribute to the Tdtomato$^+$ IHCs or SCs. Collectively, our data suggested that the progeny of the *Insm1*-expressing cells within the auditory epithelium are not as pure as previously reported (exclusively OHCs) [38]; the previously assumed "OHCs" at P0 [39] are instead potentially contaminated by 13.5%−17.9% of IHCs.

Nonetheless, obtaining pure OHCs currently is challenging, because Bcl11b, one recognized marker for embryonic OHCs [39], is also expressed in other cochlear cell types, albeit at a relatively lower level, as shown in our previous report [20]. One indirect solution might be to subtract the IHCs from the total HCs, for instance, in addition to labeling all HCs (both IHCs and OHCs) with Tdtomato by using $Atoh1^{P2A\text{-}Tdtomato/+}$ mice [20], and IHCs could be further genetically marked by GFP.

Generation of $Fgf8^{P2A\text{-}3\times GFP/+}$ for Specifically Labeling and Sorting IHCs

We sought to generate a new and simple model that not only shows specific labeling of as many IHCs as possible but also provides a bright GFP signal to enable easy and efficient labeling and sorting of embryonic or perinatal IHCs. If such a model could be designed, the opposite of sorting OHCs could be achieved in the future by excluding IHCs (see Discussion). By exploiting the specific expression pattern of *Fgf8* in embryonic or perinatal IHCs, we generated the knock-in $Fgf8^{GFP/+}$ model by inserting a P2A-3×GFP fragment immediately before the stop codon *TAG* (Fig. 2A–C); here, 3×GFP refers to three distinct GFPs, Emerald-GFP (EmGFP), TagGFP2, and humanized *Renilla*-GFP (hrGFP) [51, 52], the use of which is expected to yield a strong GFP signal. Southern blotting results confirmed that the targeting vector was not randomly inserted into the mouse genome (Fig. 2D–E), and the WT, heterozygous knock-in (KI) $Fgf8^{GFP/+}$, and homozygous $Fgf8^{GFP/GFP}$ mice were readily distinguished using tail-DNA PCR (Fig. 2F).

Neither $Fgf8^{GFP/+}$ nor $Fgf8^{GFP/GFP}$ mice exhibited any apparent abnormality, and HC development was normal in both WT (Fig. 2G) and $Fgf8^{GFP/GFP}$ (Fig. 2H) mice. Accordingly, no statistical difference was measured in the ABR thresholds at any tested frequency among WT, $Fgf8^{GFP/+}$, and $Fgf8^{GFP/GFP}$ mice at P42 ($n = 3$ for WT and $Fgf8^{GFP/+}$, $n = 4$ for $Fgf8^{GFP/GFP}$; Fig. 2I). Moreover, the ABR wave I amplitude, which reflects the synchronized output arising in the auditory nerve, did not exhibit significant differences at 8, 16, and 32 kHz (Fig. 2J–L). Collectively, these results confirmed that our genetic design did not affect the endogenous expression of *Fgf8*. Thus, we expect the $Fgf8^{GFP/+}$ mouse strain to serve as a powerful genetic tool and the GFP expression to faithfully recapitulate the *Fgf8* expression pattern, as confirmed by the findings described below.

GFP Expression is Detectable in Embryonic *Fgf8*+ Cell Populations

To verify that GFP expression matches the endogenous *Fgf8* expression *in vivo*, we first briefly characterized the GFP expression pattern in $Fgf8^{GFP/+}$ mouse embryos at three ages: E9.5, E11.5, and E12.5. At E9.5, GFP was detected in the isthmic organizer (ISO), anterior neural ridge (ANR), and branchial arch (BA) (Fig. S2A–A'), which agrees with previously-reported *Fgf8* expression [53]. In these three regions, GFP expression became relatively stronger by E11.5 (Fig. S2B–B') and was maintained at E12.5 (Fig. S2C–C'), and high GFP expression was also detected in the apical

ectodermal ridge (AER), which is a distal thickening of the ectodermal jacket of the limb bud (yellow arrows in Fig. S2B' and S2C'), in agreement with previous studies [54, 55]. Together, these results supported the conclusion that GFP expression faithfully reflects the *Fgf8* expression pattern in our $Fgf8^{GFP/+}$ mouse model.

We further characterized the GFP expression pattern in embryonic cochleae from $Fgf8^{GFP/+}$ mice. *Fgf8* expression is turned on as early as the emergence of IHCs in a basal-to-apical gradient, and *Fgf8* is expressed exclusively in IHCs [43, 56]. E14.5 was the earliest age at which faint GFP expression could be detected in nascent cochlear IHCs expressing Myo7a in the basal turn (Fig. 3A–A'), and at E15.5, GFP expression further extended to IHCs in the middle turn (Fig. 3B–B'). Consistent with the general base-to-apex HC developmental gradient, the GFP level in middle-turn IHCs was lower than that in basal IHCs at E15.5 (Fig. 3C–D'). Notably, GFP was not detected in the sensory progenitors in the apical turn that had not yet started IHC differentiation at this stage (dotted line in Fig. 3B). Here, all $Myo7a^+$ IHCs were GFP^+ and *vice versa*, although the GFP levels varied among different IHCs within the same region (compare cells indicated by arrows and arrowheads in Fig. 3C–C'). Lastly, the results of smFISH analysis of *Fgf8* at E15.5 (Fig. 3E) confirmed that *Fgf8* mRNA was primarily expressed in basal IHCs and not in apical IHCs (Fig. 3F and G). Collectively, our data revealed that GFP expression matched the endogenous *Fgf8* expression in the cochlea and other tissues at embryonic ages.

GFP Expression is High in All IHCs Across Entire Cochlear Turns at P0, but Declines Rapidly within the First Postnatal Week and Becomes Undetectable by P16

Next, we characterized the GFP expression in the cochlear IHCs of $Fgf8^{GFP/+}$ mice at P0. Fgf8 is strongly expressed in all cochlear IHCs across the basal, middle, and apical turns [56]. Accordingly, whole-mount dual labeling for the HC marker Myo7a and GFP confirmed that GFP was highly expressed in all IHCs (Fig. 4A–A'). However, unlike at E15.5, the basal-to-apical gradient of GFP expression no longer existed, although the GFP levels again varied among different IHCs within the same region (compare cells indicated by yellow and white arrows in Fig. 4B–B'). Moreover, dual-labeling for GFP and Myo7a in cryosections confirmed that GFP was expressed in all IHCs, and no GFP^+ OHCs or SCs were detected at P0 in any examined sample (Fig. 4C–D'). Lastly, *Fgf8* smFISH was again applied to cochlear samples to assess the overlap between *Fgf8* and GFP expression in IHCs at P0, which revealed that in both cryosection (Fig. 4E–F) and whole-mount (Fig. 4G–H) samples, *Fgf8* mRNA, as expected, was strongly and exclusively expressed in all IHCs.

To determine when GFP expression declines at postnatal ages, we characterized the expression in cochlear samples from $Fgf8^{GFP/+}$ mice at P7, P12, and P16. Relative to the expression level in IHCs at P0 (Fig. 4), GFP expression decreased but was still confined to all IHCs at all turns at P7 (Fig. S3A–C'). The GFP level in the cochlear IHCs further dropped by P12 and was only detectable, albeit extremely weakly, in the most apical IHCs (Fig. S3D–D'). Lastly, by P16, no GFP could be detected in any of the IHCs (Fig. S3E–E'). Altogether, our results showed that GFP expression rapidly declines after P7 along the IHC differentiation trajectory, and, furthermore, confirmed again that the expression pattern of GFP matches that of *Fgf8* because *Fgf8* expression is ultimately turned off in fully mature IHCs [26, 41, 42].

Pure IHCs can be Obtained from $Fgf8^{GFP/+}$ Cochleae at E15.5 and P1

To clearly demonstrate the power of our $Fgf8^{GFP/+}$ model as a tool for obtaining pure embryonic and neonatal IHCs, we dissected out the cochlear sensory epithelium at E15.5 and P1 separately, digested the tissue, prepared single-cell suspensions, and then subjected them to fluorescence-activated cell sorting (FACS) (Fig. 5A). Because of the heterogeneity of GFP levels among IHCs, both GFP^{high} and GFP^{low} cells were sorted (green circle in Fig. 5A). Three replicates were used per age and ~50 GFP+ cells were included in each replicate. We sought to verify the purity of the IHCs at E15.5 and P1 by applying qPCR assays with the IHC marker *Otoferlin* [35], the pan-HC marker *Myo6* [24], the SGN marker *Mafb* [57], and the SC/glial-cell marker *Sox10* [31]. We predicted that if the IHCs were highly pure, we would find significant enrichment of *Otoferlin* and *Myo6* and marked depletion of *Mafb* and *Sox10*.

Our prediction was confirmed by the qPCR results: *Otoferlin* and *Myo6* showed a fold-enrichment of 208.8 ± 74.4 and 18.5 ± 2.2 in IHCs at E15.5 relative to total RNA obtained from the P1 inner ear (P1_Total RNA) (Fig. 5B, C), whereas *Mafb* and *Sox10* showed a fold-depletion of 1138.0 ± 52.6 and 264.0 ± 1.2 relative to, respectively, SGNs at P1 (P1_SGNs) and glial cells at P7 (P7_Glial cells) (Fig. 5D, E). P1_Total RNA, P1_SGNs, and P7_Glial cells were obtained from our previous study [31]. We also measured a similar enrichment of *Otoferlin* and *Myo6* and depletion of *Mafb* and *Sox10* in IHCs at P1 (Fig. 5F–I). Moreover, the higher enrichment of *Otoferlin* in IHCs at P1 than at E15.5 agreed with the more highly differentiated state of IHCs at P1 [58]. Collectively, these results suggest that the $Fgf8^{GFP/+}$ mouse is a reliable model for obtaining highly pure IHCs by using FACS and can thus be used for multi-omic analyses in the future.

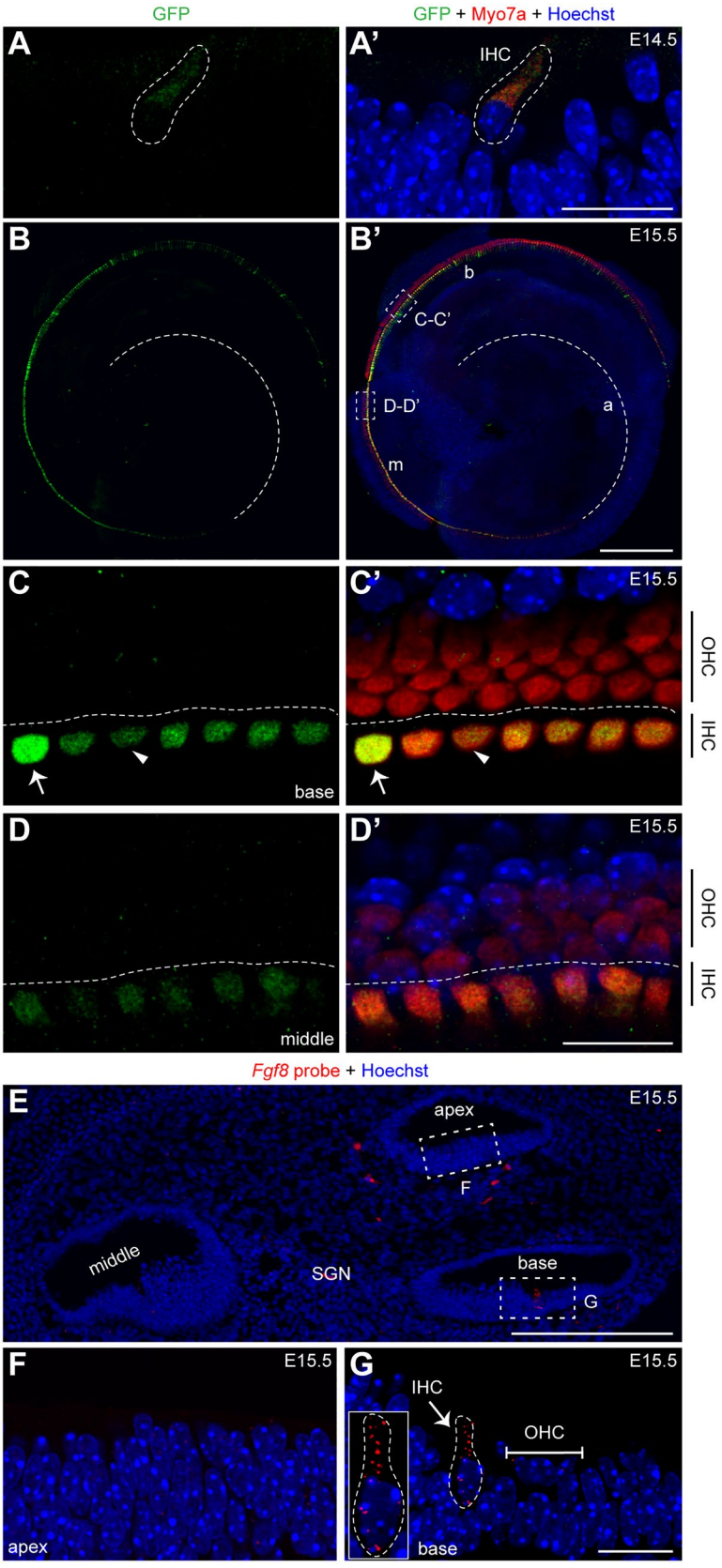

Fig. 3 GFP expression is turned on in a basal-to-apical gradient in the *Fgf8*$^{GFP/+}$ embryonic cochlea. **A–D'** Dual labeling for GFP and the HC marker Myo7a in cochlear samples at E14.5 (**A–A'**) and E15.5 (**B–D'**). White dotted circles in **A–A'**: one Myo7a^{+} IHC weakly expressing GFP. Two square regions in **B–B'** are shown at high resolution in **C–C'** and **D–D'**. Dotted lines in **B–B'**: an apical region where GFP is not expressed. Arrows and arrowheads in **C–C'**: IHCs expressing high and low levels of GFP, respectively. **E–G** *Fgf8* smFISH in cochlear cryosections at E15.5. The two square regions in **E** are shown at high resolution in **F**, apex, and **G** base. The *Fgf8* mRNA level is highest in the basal turn, consistent with the GFP expression shown in **B–B'**. Inset in **G**: the higher-magnification image of IHC is indicated by the arrow in **G**. Scale bars, 200 µm (**B'** and **E**) and 20 µm (**A'**, **D'**, **G**).

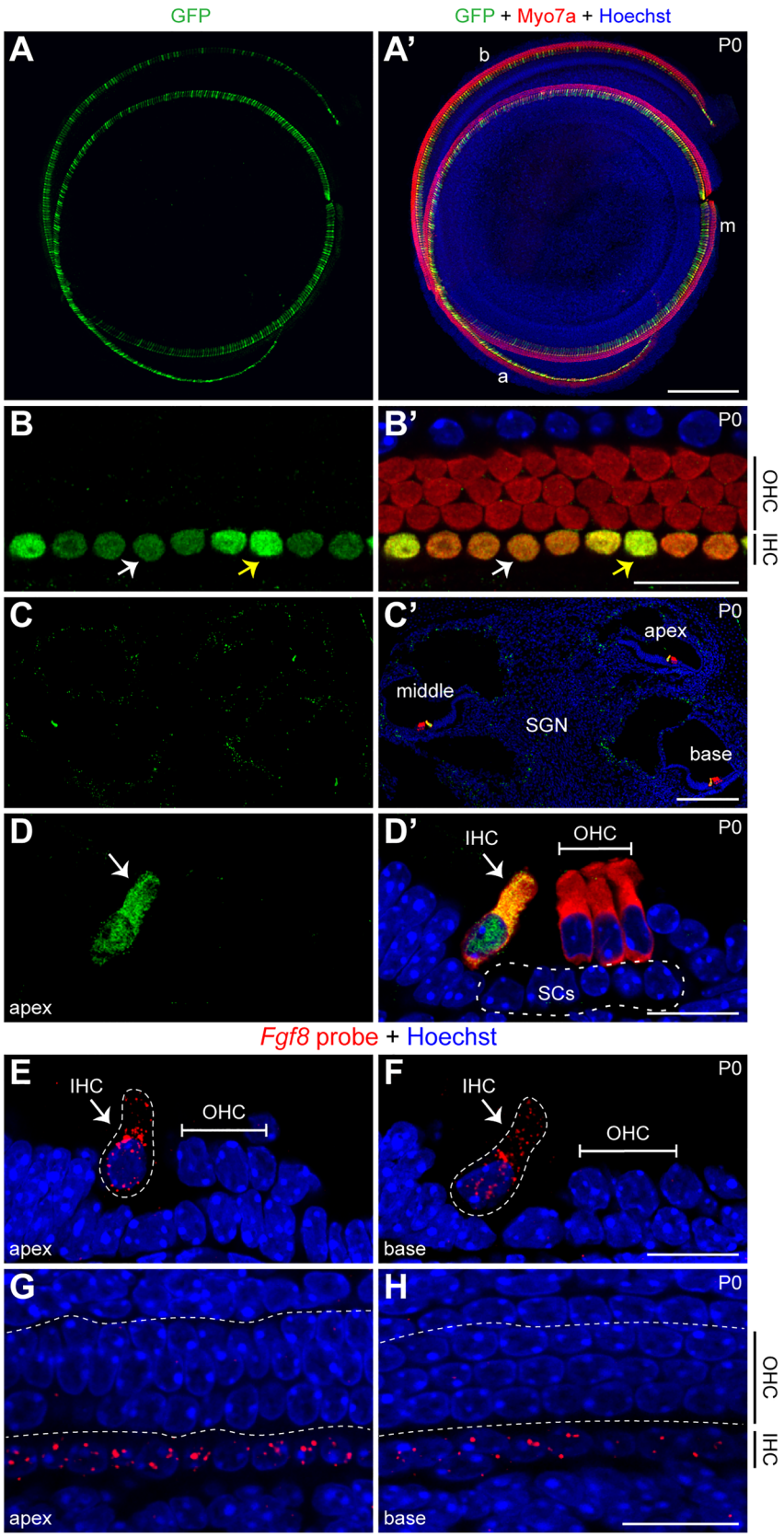

Fig. 4 GFP is strongly expressed in all IHCs of *Fgf-8*$^{GFP/+}$ mice at P0. **A–D'** Double labeling for GFP and the HC marker Myo7a (as in Fig. 3) in whole-mount (**A–B'**) and cryosection (**C–D'**) cochlear samples at P0. GFP is specifically expressed in all IHCs throughout the cochlear duct. White and yellow arrows in **B–B'**: IHCs expressing low and high levels of GFP. The apex in **C–C'** is shown at high magnification in **D–D'**. White dotted circle in **D'**: cochlear SCs (pillar and Deiters' cells). **E–H** *Fgf8* smFISH cochlear cryosections (**E** and **F**) and whole-mount (**G** and **H**) samples at P0. *Fgf8* mRNA (red puncta) is detected in IHCs but not OHCs. Scale bars, 200 μm (**A', C'**) and 20 μm (**B', D', F, H**).

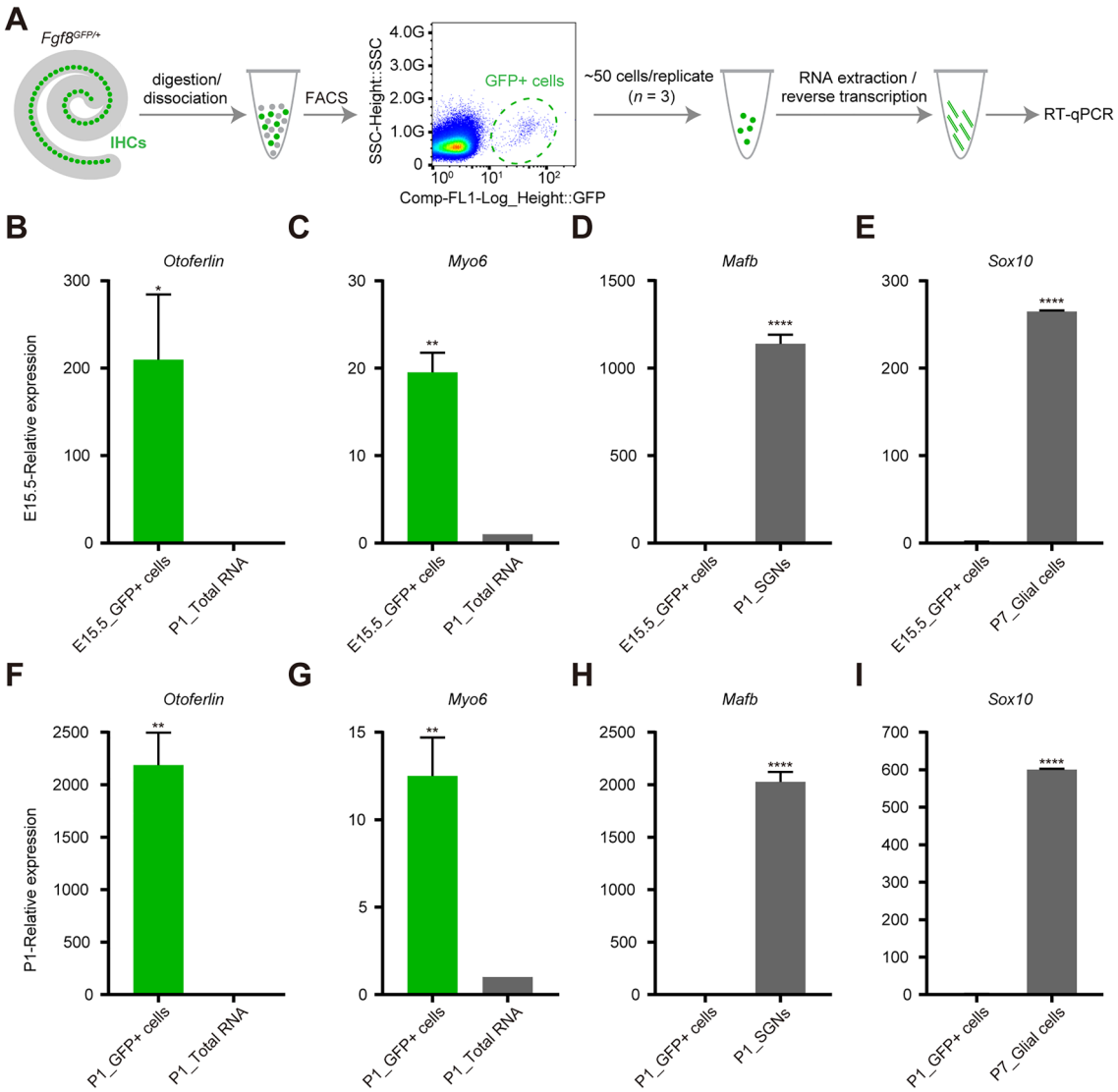

Fig. 5 IHC or HC genes are enriched but SC/glial or SGN genes are depleted in sorted GFP$^+$ IHCs at E15.5 and P1. **A** Simple illustration of sorting and qPCR analysis of GFP$^+$ IHCs from *Fgf8*$^{GFP/+}$ mice. **B–I** Sorted IHCs (~50 cells/per replicate, three biological replicates) at E15.5 (**B–E**) and P1 (**F–I**) show enrichment of the IHC gene *Otoferlin* (**B** and **F**) and the pan-HC gene *Myo6* (**C** and **G**) but depletion of the SGN gene *Mafb* (**D** and **H**) and the SC/glial-cell gene *Sox10* (**E** and **I**), relative to control cDNAs derived from entire inner ear tissues at P1 (P1_Total RNA), pure SGNs at P1 (P1_SGNs), or pure glial cells at P7 (P7_Glial cells). Data are presented as the mean ± SEM (n = 3); ****P <0.0001, **P <0.01, *P <0.05 (Student's t test).

GFP Is Detectable in Vestibular HCs at E17.5

The Fgf8 expression pattern in inner ear vestibular HCs has recently been characterized in detail [56]. Here, we briefly characterized vestibular HCs at E17.5 to reveal their GFP expression pattern, which overlapped with that of the HC marker Myo7a (Fig. S4A, A'). GFP was expressed at a higher level in the utricle and saccular HCs (yellow arrows in Fig. S4B–C'') than in the HCs in the crista ampullaris (yellow arrows in Fig. S4D–D''), GFP being undetectable in some of the HCs in the crista ampullaris (white arrows in Fig. S4D–D''). Thus, the *Fgf8*$^{GFP/+}$ model is also suitable for labeling and sorting vestibular HCs.

Discussion

Genetic Models to Specifically Label Mouse IHCs at Different Ages

Our primary goal in this study was to establish a genetic mouse model that can be used to specifically label as many IHCs as possible at both embryonic and perinatal ages. In

principle, two *Fgf8*$^{CreER/+}$ mouse lines, one in which *Fgf8* expression itself is replaced by CreER expression and *Fgf8*^{CreER} is a null allele [59], or the other in which *Fgf8* expression is intact [56], can be used to label IHCs with Tdtomato in *Fgf8*$^{CreER/+}$; Ai9/+ mice at perinatal ages, as reported previously [56]. However, two technical barriers prevent *Fgf8*$^{CreER/+}$; Ai9/+ from being suitable for conveniently labeling embryonic and perinatal cochlear IHCs: one, the delay between efficient Cre expression driven by *Fgf8* and sufficient reporter expression; and two, the dystocia invariably caused in pregnant females by embryonic exposure to tamoxifen.

Conversely, in our model, all Myo7a$^+$ IHCs were GFP$^+$ between E15.5 and P7, and the GFP expression directly reflected the temporal expression pattern of *Fgf8*. By using IHCs at E15.5 and P1 as examples, we demonstrated that the *Fgf8*$^{GFP/+}$ mouse is a powerful model for labeling and sorting highly pure IHCs. We propose that by using our model, pure IHCs between E15.5 and P4 can be sorted at the bulk or single-cell level for RNA-seq, ATAC-seq, or other multi-omic analyses. In terms of IHCs at ages between P5 and P21, it might be preferable to use *Fgf8*$^{CreER/+}$; Ai9/+ mice that are administered tamoxifen at P0 and P1 and then analyzed at different ages depending on the experimental aims. Alternatively, if the goal is to avoid exposing mice to tamoxifen at neonatal ages but still label and sort IHCs at adult ages, *vGlut3*$^{P2A\text{-}iCreER/+}$; Ai9/+ is another option [4]; for example, adult *vGlut3*$^{P2A\text{-}iCreER/+}$; Ai9/+ mice can be treated with tamoxifen at P30 to enable IHC sorting based on Tdtomato at P38, as we reported previously [4].

The Solution to Exclusively Labelling Neonatal OHCs

Prestin is specifically and persistently expressed in cochlear OHCs after its expression is turned on in these cells around P2 in a basal-to-apical gradient [3]. Therefore, cochlear OHCs at P5 or thereafter can be efficiently traced using *Prestin*$^{CreER/+}$ [3, 48]. For instance, if *Prestin*$^{CreER/+}$; Ai9/+ mice are treated with tamoxifen at various ages, including neonatal P2 and P3, juvenile P10 and P11, and adult ages of P30 and thereafter, most, if not all, OHCs should express Tdtomato at high levels one week after the tamoxifen administration. Notably, our results showed that distinct from a previous report [39], GFP$^+$/Tdtomato$^+$ cells are not pure OHCs in the *Insm1*$^{GFPCre/+}$; Ai9/+; *Atoh1*$^{EGFP/+}$ model at P0, because 13.5−17.9% of IHCs were also traced based on *Insm1*$^{GFPCre/+}$. Thus, specific labeling of cochlear OHCs at perinatal ages remains a major challenge.

How might the barrier to specifically targeting OHCs at P0 be overcome? We propose that a potential solution is the combined use of the knock-in *Atoh1*$^{P2A\text{-}Tdtomato/+}$ model [20] and the *Fgf8*$^{GFP/+}$ model. We have reported that all cochlear HCs (IHCs and OHCs) are Tdtomato+ in *Atoh1*$^{P2A\text{-}Tdtomato/+}$ mice at neonatal ages [20]. Thus, in *Fgf8*$^{GFP/+}$; *Atoh1*$^{P2A\text{-}Tdtomato/+}$ mice at P0, in principle, GFP$^+$/Tdtomato$^+$ cells would be IHCs, whereas Tdtomato$^+$/GFP$^-$ cells would be OHCs. Notably, the GFP levels are heterogeneous among IHCs at P0 (Fig. 4A–B') and thus two IHC subpopulations, GFP^{high} and GFP^{low}, are expected to be present, and the gating in FACS should be set to exclude both GFP^{high} and GFP^{low} IHCs to guarantee the purity of the OHCs of interest. The heterogeneous GFP expression level, in principle, reflects varying levels of Fgf8 expression in IHCs, but how this heterogeneous Fgf8 expression is generated remains unknown.

Application of *Fgf8*$^{GFP/+}$ in Studies on HC Regeneration *in vivo*, Particularly IHC Regeneration

Fgf8 exhibits a specific and dynamic expression pattern and plays a critical role in cochlear development [43]; therefore, *Fgf8* can serve as a reliable marker to define the IHC fate, particularly in the nascent and differentiating IHC states. To date, no suitable commercial antibodies for Fgf8 immunostaining have been available, and thus GFP is used to readily represent Fgf8 expression in the *Fgf8*$^{GFP/+}$ strain. We previously confirmed that Atoh1 overexpression alone is sufficient to convert neonatal cochlear inner border cells/inner phalangeal cells (IBCs/IPhs) into immature IHCs expressing the early pan-HC markers Myo6 and Fgf8, but not vGlut3 [45], and we recently showed that Tbx2 and Atoh1 together can further reprogram neonatal IBCs/IPhs into IHCs expressing both Myo6 and vGlut3 [26]. These new IHCs should be Fgf8$^+$, which can be verified by incorporating the *Fgf8*$^{GFP/+}$ strain into the Tbx2/Atoh1-mediated IHC regeneration. Conversely, the *Fgf8*$^{GFP/+}$ strain can also be crossed into our Atoh1/Ikzf2-mediated OHC regeneration model to confirm that the new OHC-like cells do not express Fgf8 and are GFP$^-$. In sum, we believe that *Fgf8*$^{GFP/+}$ will emerge as a powerful model for IHC-specific labeling and sorting and determining the cell fate of newly regenerated HCs, and the model will also facilitate future multi-omic studies on cochlear HC development.

Acknowledgments We thank Dr. Qian Hu from the Optical Imaging Facility of the ION for support with image analysis, and Ms. Qian Liu from the Department of Embryology of the ION animal center for helping us in transplanting zygotes into pseudopregnant female mice. This work was funded by the National Key R&D Program of China (2021YFA1101804), the Strategic Priority Research Program of the Chinese Academy of Science (XDB32060100), the National Natural Science Foundation of China (91949119, 82101212, and 82101209), a Shanghai Municipal Science and Technology Major Project (2018SHZDZX05), the Science and Technology Commission of Shanghai Municipality (21ZR1440200), and the Shanghai Sailing Program (20YF1426400).

Conflict of interest The authors declare that there are no conflicts of interest.

References

1. Wang S, Lee MP, Jones S, Liu J, Waldhaus J. Mapping the regulatory landscape of auditory hair cells from single-cell multi-omics data. Genome Res 2021, 31: 1885–1899.
2. Yang H, Gan J, Xie X, Deng M, Feng L, Chen X. Gfi1-Cre knock-in mouse line: A tool for inner ear hair cell-specific gene deletion. Genesis 2010, 48: 400–406.
3. Fang J, Zhang WC, Yamashita T, Gao J, Zhu MS, Zuo J. Outer hair cell-specific prestin-CreERT2 knockin mouse lines. Genesis 2012, 50: 124–131.
4. Li C, Shu Y, Wang G, Zhang H, Lu Y, Li X, *et al*. Characterizing a novel vGlut3-P2A-iCreER knockin mouse strain in cochlea. Hear Res 2018, 364: 12–24.
5. Tang Q, Xu M, Xu J, Xie X, Yang H, Gan L. Gfi1-GCE inducible Cre line for hair cell-specific gene manipulation in mouse inner ear. Genesis 2019, 57: e23304.
6. Tao L, Yu HV, Llamas J, Trecek T, Wang X, Stojanova Z, *et al*. Enhancer decommissioning imposes an epigenetic barrier to sensory hair cell regeneration. Dev Cell 2021, 56: 2471-2485.e5.
7. Yu HV, Tao L, Llamas J, Wang X, Nguyen JD, Trecek T, *et al*. POU4F3 pioneer activity enables ATOH1 to drive diverse mechanoreceptor differentiation through a feed-forward epigenetic mechanism. Proc Natl Acad Sci U S A 2021, 118: e2105137118.
8. Jan TA, Eltawil Y, Ling AH, Chen L, Ellwanger DC, Heller S, *et al*. Spatiotemporal dynamics of inner ear sensory and non-sensory cells revealed by single-cell transcriptomics. Cell Rep 2021, 36: 109358.
9. Xu J, Li J, Zhang T, Jiang H, Ramakrishnan A, Fritzsch B, *et al*. Chromatin remodelers and lineage-specific factors interact to target enhancers to establish proneurosensory fate within otic ectoderm. Proc Natl Acad Sci U S A 2021, 118: e2025196118.
10. Sun Y, Wang L, Zhu T, Wu B, Wang G, Luo Z, *et al*. Single-cell transcriptomic landscapes of the otic neuronal lineage at multiple early embryonic ages. Cell Rep 2022, 38: 110542.
11. Montcouquiol M, Kelley MW. Development and patterning of the cochlea: From convergent extension to planar polarity. Cold Spring Harb Perspect Med 2020, 10: a033266.
12. Groves AK, Zhang KD, Fekete DM. The genetics of hair cell development and regeneration. Annu Rev Neurosci 2013, 36: 361–381.
13. Wu DK, Kelley MW. Molecular mechanisms of inner ear development. Cold Spring Harb Perspect Biol 2012, 4: a008409.
14. Luo Z, Zhang J, Qiao L, Lu F, Liu Z. Mapping genome-wide binding sites of Prox1 in mouse cochlea using the CUT&RUN approach. Neurosci Bull 2021, 37: 1703–1707.
15. Matei V, Pauley S, Kaing S, Rowitch D, Beisel KW, Morris K, *et al*. Smaller inner ear sensory epithelia in Neurog 1 null mice are related to earlier hair cell cycle exit. Dev Dyn 2005, 234: 633–650.
16. Yang H, Xie X, Deng M, Chen X, Gan L. Generation and characterization of Atoh1-Cre knock-in mouse line. Genesis 2010, 48: 407–413.
17. Driver EC, Sillers L, Coate TM, Rose MF, Kelley MW. The Atoh1-lineage gives rise to hair cells and supporting cells within the mammalian cochlea. Dev Biol 2013, 376: 86–98.
18. Li S, Fan T, Li C, Wang Y, Li J, Liu Z. Fate-mapping analysis of cochlear cells expressing Atoh1 mRNA via a new Atoh1$^{3*HA\text{-}P2A\text{-}Cre}$ knockin mouse strain. Dev Dyn 2022, 251: 1156–1174.
19. Tateya T, Sakamoto S, Ishidate F, Hirashima T, Imayoshi I, Kageyama R. Three-dimensional live imaging of Atoh1 reveals the dynamics of hair cell induction and organization in the developing cochlea. Development 2019, 146: dev177881.
20. Luo Z, Du Y, Li S, Zhang H, Shu M, Zhang D, *et al*. Three distinct *Atoh1* enhancers cooperate for sound receptor hair cell development. Proc Natl Acad Sci U S A 2022, 119: e2119850119.
21. Bermingham NA, Hassan BA, Price SD, Vollrath MA, Ben-Arie N, Eatock RA, *et al*. Math1: An essential gene for the generation of inner ear hair cells. Science 1999, 284: 1837–1841.
22. Woods C, Montcouquiol M, Kelley MW. Math1 regulates development of the sensory epithelium in the mammalian cochlea. Nat Neurosci 2004, 7: 1310–1318.
23. Wang G, Li C, He S, Liu Z. Mosaic CRISPR-stop enables rapid phenotyping of nonsense mutations in essential genes. Development 2021, 148: dev196899.
24. Avraham KB, Hasson T, Steel KP, Kingsley DM, Russell LB, Mooseker MS, *et al*. The mouse Snell's waltzer deafness gene encodes an unconventional myosin required for structural integrity of inner ear hair cells. Nat Genet 1995, 11: 369–375.
25. Li Y, Liu H, Giffen KP, Chen L, Beisel KW, He DZZ. Transcriptomes of cochlear inner and outer hair cells from adult mice. Sci Data 2018, 5: 180199.
26. Bi Z, Li X, Ren M, Gu Y, Zhu T, Li S, *et al*. Development and transdifferentiation into inner hair cells require Tbx2. Natl Sci Rev 2022, 9: nwac156.
27. Xu Z, Tu S, Pass C, Zhang Y, Liu H, Diers J, *et al*. Profiling mouse cochlear cell maturation using 10× Genomics single-cell transcriptomics. Front Cell Neurosci 2022, 16: 962106.
28. Zheng J, Shen W, He DZ, Long KB, Madison LD, Dallos P. Prestin is the motor protein of cochlear outer hair cells. Nature 2000, 405: 149–155.
29. Liberman MC, Gao J, He DZZ, Wu X, Jia S, Zuo J. Prestin is required for electromotility of the outer hair cell and for the cochlear amplifier. Nature 2002, 419: 300–304.
30. Li J, Liu S, Song C, Zhu T, Zhao Z, Sun W, *et al*. Prestin-mediated frequency selectivity does not cover ultrahigh frequencies in mice. Neurosci Bull 2022, 38: 769–784.
31. Li C, Li X, Bi Z, Sugino K, Wang G, Zhu T, *et al*. Comprehensive transcriptome analysis of cochlear spiral ganglion neurons at multiple ages. Elife 2020, 9: e50491.
32. Petitpré C, Wu H, Sharma A, Tokarska A, Fontanet P, Wang Y, *et al*. Neuronal heterogeneity and stereotyped connectivity in the auditory afferent system. Nat Commun 2018, 9: 3691.
33. Shrestha BR, Chia C, Wu L, Kujawa SG, Liberman MC, Goodrich LV. Sensory neuron diversity in the inner ear is shaped by activity. Cell 2018, 174: 1229-1246.e17.
34. Sun S, Babola T, Pregernig G, So KS, Nguyen M, Su SSM, *et al*. Hair cell mechanotransduction regulates spontaneous activity and spiral ganglion subtype specification in the auditory system. Cell 2018, 174: 1247-1263.e15.
35. Roux I, Safieddine S, Nouvian R, Grati M, Simmler MC, Bahloul A, *et al*. Otoferlin, defective in a human deafness form, is essential for exocytosis at the auditory ribbon synapse. Cell 2006, 127: 277–289.
36. Seal RP, Akil O, Yi E, Weber CM, Grant L, Yoo J, *et al*. Sensorineural deafness and seizures in mice lacking vesicular glutamate transporter 3. Neuron 2008, 57: 263–275.
37. Ruel J, Emery S, Nouvian R, Bersot T, Amilhon B, Van Rybroek JM, *et al*. Impairment of SLC17A8 encoding vesicular glutamate transporter-3, VGLUT3, underlies nonsyndromic deafness DFNA25 and inner hair cell dysfunction in null mice. Am J Hum Genet 2008, 83: 278–292.
38. Lorenzen SM, Duggan A, Osipovich AB, Magnuson MA, García-Añoveros J. Insm1 promotes neurogenic proliferation in delaminated otic progenitors. Mech Dev 2015, 138(Pt 3): 233–245.
39. Wiwatpanit T, Lorenzen SM, Cantú JA, Foo CZ, Hogan AK, Márquez F, *et al*. Trans-differentiation of outer hair cells into inner hair cells in the absence of INSM1. Nature 2018, 563: 691–695.

40. Chessum L, Matern MS, Kelly MC, Johnson SL, Ogawa Y, Milon B, *et al*. Helios is a key transcriptional regulator of outer hair cell maturation. Nature 2018, 563: 696–700.
41. García-Añoveros J, Clancy JC, Foo CZ, García-Gómez I, Zhou Y, Homma K, *et al*. Tbx2 is a master regulator of inner versus outer hair cell differentiation. Nature 2022, 605: 298–303.
42. Kaiser M, Lüdtke TH, Deuper L, Rudat C, Christoffels VM, Kispert A, *et al*. TBX2 specifies and maintains inner hair and supporting cell fate in the Organ of Corti. Nat Commun 2022, 13: 7628.
43. Jacques BE, Montcouquiol ME, Layman EM, Lewandoski M, Kelley MW. Fgf8 induces pillar cell fate and regulates cellular patterning in the mammalian cochlea. Development 2007, 134: 3021–3029.
44. Quadros RM, Miura H, Harms DW, Akatsuka H, Sato T, Aida T, *et al*. Easi-CRISPR: A robust method for one-step generation of mice carrying conditional and insertion alleles using long ssDNA donors and CRISPR ribonucleoproteins. Genome Biol 2017, 18: 92.
45. Liu Z, Fang J, Dearman J, Zhang L, Zuo J. *In vivo* generation of immature inner hair cells in neonatal mouse cochleae by ectopic Atoh1 expression. PLoS One 2014, 9: e89377.
46. Osipovich AB, Long Q, Manduchi E, Gangula R, Hipkens SB, Schneider J, *et al*. Insm1 promotes endocrine cell differentiation by modulating the expression of a network of genes that includes Neurog3 and Ripply3. Development 2014, 141: 2939–2949.
47. Tang X, Gao J, Jia X, Zhao W, Zhang Y, Pan W, *et al*. Bipotent progenitors as embryonic origin of retinal stem cells. J Cell Biol 2017, 216: 1833–1847.
48. Sun S, Li S, Luo Z, Ren M, He S, Wang G, *et al*. Dual expression of Atoh1 and Ikzf2 promotes transformation of adult cochlear supporting cells into outer hair cells. Elife 2021, 10: e66547.
49. Sun Y, Zhang Y, Zhang D, Wang G, Song L, Liu Z. *In vivo* CRISPR-Cas9-mediated DNA chop identifies a cochlear outer hair cell-specific enhancer. FASEB J 2022, 36: e22233.
50. Rose MF, Ren J, Ahmad KA, Chao HT, Klisch TJ, Flora A, *et al*. Math1 is essential for the development of hindbrain neurons critical for perinatal breathing. Neuron 2009, 64: 341–354.
51. Li X, Yu B, Sun Q, Zhang Y, Ren M, Zhang X, *et al*. Generation of a whole-brain atlas for the cholinergic system and mesoscopic projectome analysis of basal forebrain cholinergic neurons. Proc Natl Acad Sci U S A 2018, 115: 415–420.
52. Li X, Bi Z, Sun Y, Li C, Li Y, Liu Z. *In vivo* ectopic Ngn1 and Neurod1 convert neonatal cochlear glial cells into spiral ganglion neurons. FASEB J 2020, 34: 4764–4782.
53. Compagnucci C, Debiais-Thibaud M, Coolen M, Fish J, Griffin JN, Bertocchini F, *et al*. Pattern and polarity in the development and evolution of the gnathostome jaw: Both conservation and heterotopy in the branchial arches of the shark, *Scyliorhinus canicula*. Dev Biol 2013, 377: 428–448.
54. Farin HF, Lüdtke TH, Schmidt MK, Placzko S, Schuster-Gossler K, Petry M, *et al*. Tbx2 terminates shh/fgf signaling in the developing mouse limb bud by direct repression of gremlin1. PLoS Genet 2013, 9: e1003467.
55. Lewandoski M, Sun X, Martin GR. Fgf8 signalling from the AER is essential for normal limb development. Nat Genet 2000, 26: 460–463.
56. Ratzan EM, Moon AM, Deans MR. *Fgf8* genetic labeling reveals the early specification of vestibular hair cell type in mouse utricle. Development 2020, 147: dev192849.
57. Yu WM, Appler JM, Kim YH, Nishitani AM, Holt JR, Goodrich LV. A Gata3-Mafb transcriptional network directs post-synaptic differentiation in synapses specialized for hearing. Elife 2013, 2: e01341.
58. Kolla L, Kelly MC, Mann ZF, Anaya-Rocha A, Ellis K, Lemons A, *et al*. Characterization of the development of the mouse cochlear epithelium at the single cell level. Nat Commun 2020, 11: 2389.
59. Hoch RV, Clarke JA, Rubenstein JL. Fgf signaling controls the telencephalic distribution of Fgf-expressing progenitors generated in the rostral patterning center. Neural Dev 2015, 10: 8.